Journal of Membrane Science 702 (2024) 122799

Contents lists available at ScienceDirect

Journal of Membrane Science

journal homepage: www.elsevier.com/locate/memsci

Stabilizing graphene oxide with complementary nanosheets for robust membranes with high flux

Rui Li [a,b,1], Xiaoquan Feng [a,1], Huixian Wang [b], Donglai Peng [a,c], Shaochong Cao [a], Jingtao Wang [a], Yatao Zhang [a,*], Yong Wang [d,**]

[a] School of Chemical Engineering, Zhengzhou University, Zhengzhou, 450001, China
[b] School of Material Science and Engineering, North China University of Water Resources and Electric Power, Zhengzhou, 450046, China
[c] School of Materials and Chemical Engineering, Zhengzhou University of Light Industry, Zhengzhou, 450002, China
[d] School of Energy and Environment, Southeast University, Nanjing, 210096, Jiangsu, China

ARTICLE INFO

Keywords:
Graphene oxide
Complementary nanosheets
Ionic covalent organic frameworks
Laminar assembles
High water permeance

ABSTRACT

Laminar assembles of graphene oxide (GO) are receiving tremendous attention for their interesting nanofluidic behaviors, but suffer from structural instability and frustrated mass transfer. Herein, we stabilize GO assembles by "complementary nanosheets", and thus obtain highly robust and permeable membranes. Self-exfoliated nanosheets of ionic covalent organic frameworks (iCONs) are intercalated into GO nanosheets. GO and iCONs are physicochemically complementary as they carry opposite charges and hydrogen bonds acceptors and donors, respectively. Upon mixing, they form laminar assembles locked by electrostatic attraction and hydrogen bonds, suppressing swelling in water. Moreover, simulation and experimental results reveal that iCONs expands the interlayer distance and provides additional mass-transport paths. Consequently, the GO/iCONs membranes exhibit ultra-high water permeance up to 11-fold larger than that of pure GO membranes. This work provides a controllable route to stabilize GO assembles, and develops new membranes using complementary two-dimensional structures as building blocks.

1. Introduction

Graphene oxide based (GO-based) laminar membranes with diverse functional groups and adjustable architecture have aroused increasing attention [1–3]. However, the actual feasibility of GO-based membranes has been greatly impeded by structural vulnerability and low water permeance [4,5]. The superb hydrophilicity of GO laminates makes them tend to absorb water and swell, resulting in an overlarge interlayer spacing and greatly influencing anticipative performance [6,7]. Hence, solving the instability and low permeance issues of GO-based membranes is expected to break through the obstacles for GO-based laminar membranes.

Adequate stability is imperative to stabilize transmembrane nanofluidic transport and forecast performance in practice. Recently, massive endeavors have been made to maintain the stability of GO-based laminar membranes, containing chemical and physical approaches. The existing strategies mainly comprise of crosslinking GO nanolaminates with guest materials, including different dimensional materials, molecules and ions. The crosslinkers are usually inserted or *in-situ* grown between host GO nanolaminates to maintain lamellar architecture via introducing one or several attractive forces [8,9]. Besides, the chemical reduction is capable of improving the robustness of GO-related membranes in water by means of hydroiodic acid or hydrazine [10,11]. Utilizing electrostatic attraction or intermolecular force has been supposed as efficacious strategies to significantly enhance stability of GO-based membranes [12,13]. Although a lot of endeavors have been made in advancing water robustness of GO-based membranes by above-mentioned methods, it still confronts the issues of occupying channels and weakening interaction forces of GO-based membranes, enabling water molecules difficult enter into transport path, and thus leading to unsatisfactory water permeance. In view of the impermeability of GO laminates to aqueous molecules, how to improve water permeance of GO-based membranes is also our focus point. One strategy is making pores in GO laminates prior to self-assembly to enhance water permeance [14]. Another effective

* Corresponding author.
** Corresponding author.
E-mail addresses: zhangyatao@zzu.edu.cn (Y. Zhang), yongwang@seu.edu.cn (Y. Wang).
[1] These authors contributed equally to this work.

https://doi.org/10.1016/j.memsci.2024.122799
Received 5 February 2024; Received in revised form 11 April 2024; Accepted 18 April 2024
Available online 20 April 2024

strategy is to enlarge the interlayer spacing amid GO nanosheets, yet this augment is greatly hampered by the long and tortuous transmission paths of GO nanosheets without holes in the plane [15]. With regards to horizontally self-assembly GO-based membranes, cracks or gaps among GO laminates are the sole vertical transport channels which largely influence the mass transmission rate. Hence, it is expected that the porous materials possessing multidimensional channels composited with GO nanosheets are introduced to improve water flux and strengthen stability.

2D covalent organic framework (COF) nanosheets are constructed by symmetrically ordered organic linkers by strong covalent bonds [16]. Equipped with well-organized pores and modifiable structures, 2D COF nanosheets may afford vertical transport pathways via in-plane pores for small molecules, rather than the confined and tortuous diffusion routes among layers [17]. For instance, pliable and free-standing pure COF membranes were constructed by the liquid-liquid interface-restrained reaction at ambient temperature, which exhibited a high permeance as well as a high retention of brilliant blue [18]. Nevertheless, inferior processability of COF nanosheets is still the primary weakness, hindering the preparation of a complete continuous COF films. Based on the above issues, it is intriguing to integrate the elasticity of GO nanosheets with the virtues of COFs laminates to achieve high-performance continuous mixed nanolaminates. Thin COF nanosheets can not only efficiently customize the interlayer spacing between GO laminates [19], but possess completely organic composition, which are in favor of preferable compatibility and seamless assembly with GO-based laminar membranes [20]. Several studies have reported COFs nanosheets as a spacer to tune the interlayer spacing of graphene nanosheets for enhancing permeance [21]. However, the major obstacles exist in the deficiency of water stability and COF nanosheets exfoliated into thin layers.

In this study, self-exfoliated guanidinium-based ionic covalent organic nanosheets were successfully synthesized, which possessed superb water stability and exhibited easy assembly with GO nanosheets for constructing laminar membranes. Positively charged guanidinium units make interlayer repulsion self-exfoliate into less layered COF nanosheets and demonstrate a remarkable stability in aqueous solution [22]. The existence of iCONs amid in GO nanosheets avails to enhance structural robustness in water, which is primarily ascribed to hydrogen bonding interaction and electrostatic attraction between guanidinium units within iCONs and oxygen-containing functional groups within GO nanolaminates. Meanwhile, the fabricated iCONs/GO membranes possess ultra-high permeance as well as outstanding sieving capacity for dyes and salts, greatly surpassing most of pure GO-based membranes. Moreover, the inherent antimicrobial property endows the composite membranes fairly dominant for any water-related practical applications. Finally, we estimate the stability of the fabricated membranes and theoretically explain transport property of water molecules and diverse solutes in virtue of density functional theory (DFT) and molecular dynamics (MD) simulations through the pure GO and iCONs/GO membranes. This work details the introduction of COF nanosheets for promoting the property of GO-based membranes, affording insights into the design of complementary water-based treatment membranes.

2. Methods

2.1. Materials and chemicals

Triaminoguanidinium chloride (TGCl) and 1,3,5-triformylphloroglucinol (Tp) were bought from Tensus Bio-tech Co., Ltd (Shanghai, China). The solvents including dimethylacetamide (DMAC) and acetone were purchased from Aladdin Reagent Co., Ltd (Shanghai, China). Eriochrome black T (EBT), methyl blue (MB), reactive black 5 (RB5), methyl orange (MO) and direct red23 (DR23) were also bought from Aladdin Reagent Co., Ltd (Shanghai, China). Nylon microfiltration substrates (0.22 μm) were provided by Jinteng Experimental Equipment Co., Ltd (Tianjin, China). GO powder was synthesized according to our previous published reports [23], referring to supporting information for specific steps.

2.2. Synthesis of iCONs

The iCONs ($TpTG_{Cl}$) were synthesized based on Schiff base reaction between 0.2 mmol TGCl and 0.2 mmol Tp in a sealed Pyrex tube adopting water and dioxane as solvents. The mixtures were decanted into Pyrex tube and then sonicated for 20 min. Afterwards, degasification was conducted through freeze-pump-thaw procedures repeated three times utilizing liquid N_2 and then the Pyrex tube was sealed by the aid of vacuum. The mixtures were permitted to achieve room temperature and subsequently retained at 120 °C for 72 h. Eventually, the product was rinsed with DMAC, water, and acetone three times and dried at 100 °C for overnight to acquire in ~75 % isolated yield.

2.3. Fabrication of GO/iCONs composite membranes

Prior to membranes fabrication, the dispersion solution of GO and iCONs were prepared, respectively. Firstly, 10 mg iCONs were dispersed into 100 mL DI water (0.1 mg mL^{-1}) and treated by ultrasonic apparatus for 20 min. Then the mixture was centrifuged at 2000 rpm for 10 min to get rid of the bulks, and the suspension was collected as the finally iCONs dispersion with a concentration of about 0.045 mg mL^{-1}. Meanwhile, GO aqueous dispersion (0.1 mg mL^{-1}) was prepared also adopting bath sonication for 20 min. Afterwards, the GO/iCONs composite membranes were fabricated by a vacuum-assisted method. In detail, a blended solution of iCONs and GO was sonicated for another 20 min before being filtered onto nylon substrates (13.85 cm^2 area) to acquire homogeneous and continuous membranes. The membranes were fabricated with a GO/iCONs mass ratio varied from 8:1 to 1:1. GO membranes were also fabricated as a contrast. 1 mL of GO aqueous solution diluted to 10 mL was filtered without the existence of iCONs. It should be noted that GO loading on all membranes had the equal loading at 0.1 mg. Once the filtration finished, the as-fabricated membranes were dried in a fume hood for 12 h prior to performance test. The different mass ratio of GO to iCONs (8:1, 4:1, 2:1, 4:3, 1:1) were assembled into the composited membranes and named as M1, M2, M3, M4 and M5, as illustrated in Table S2.

2.4. Characterization of iCONs and GO/iCONs membranes

The as-synthesized iCONs powder was characterized by X-ray diffraction (XRD) in the 2θ range varied from 5° to 15° to verify the crystal structure. The chemical structure of iCONs powder and GO/iCONs membranes were respectively analyzed through Fourier transform infrared spectroscopies (FTIR) and attenuated total reflection Fourier transform infrared (ATR-FTIR) spectrometer. The morphology of iCONs was observed via transmission electron microscopy and scanning electron microscope (SEM). The surface area and pore size distribution curve were acquired from the adsorption data using the Langmuir and Brunauer-Emmett-Teller (BET) method and the adsorptive branch based on the non-local density functional theory (NLDFT) protocol. The thermal stability of iCONs powder and the as-prepared membranes were measured by thermogravimetric analysis (TGA). The rate of heat is 10 °C/min until to 800 °C in a flowing nitrogen atmosphere. The surface chemical components of GO/iCONs membranes were explored with X-ray photoelectron spectroscopy (XPS) analyses. To explore the surface hydrophilicity of membranes, static water contact angles (WCA) were measured with an EasyDrop contact angle device and software (Kruss, Germany). Zeta potentials of the membranes were measured via a SurPASS™ 3 electrokinetic analyzer (Anton Paar, Graz, Austria). 1.0 mM KCl solution was selected as the background electrolyte. The pH values varied over a range of 3–10 at room temperature. The detailed models and working parameters of the aforementioned characterizations were

the same as our previous report, except otherwise noted [24]. Additionally, the approximately interlayer spacing was calculated on the basis of the Bragg equation:

$$2dsin\theta = n\lambda \quad (1)$$

where d refers to the d-spacing, θ represents the diffraction angle, n expressed diffraction series is 1, λ is the wavelength of the Cu X-ray beam (0.15406 nm).

2.5. Filtration performance

The permeance and separation property of GO/iCONs membranes were assessed through a cross-flow filtration setup at room temperature. Firstly, the membranes were placed into two same cross-flow filtration cells with an efficacious area of 7.065 cm^2. Then, the membranes were pre-pressurized at 2 bar at least 1 h to guarantee that the membranes attained a stable status. Afterwards, the performance test was conducted at 1 bar. Water permeance (WP) of the membranes were counted as follows:

$$WP = \frac{\Delta V}{A_m \times \Delta t \times \Delta P} \quad (2)$$

Where ΔV, A_m, Δt, and ΔP respectively represent the volume of collected permeate (L), the effective surface area (cm^2), the filtration time (h), and the *trans*-membrane pressure (bar).

The salts rejections (R_s, Na_2SO_4, $MgSO_4$, NaCl, $MgCl_2$, 1 g L^{-1}) and dyes rejections (R_d, EBT, MB, RB5, DR23, MO, 0.2 g L^{-1}) were calculated at 1 bar based on the following equation:

$$R = \left(1 - \frac{C_p}{C_f}\right) \times 100\% \quad (3)$$

Where C_f and C_p are the concentrations in the feed and permeate, respectively. The conductivity of the salt solution was measured by adopting a conductivity meter (DDS-11A). The concentrations of dyes were quantified using UV–Vis spectrophotometry. For dye/salt or dye/dye hybrid solution, equal volume of 100 ppm dye solution and 1000 ppm salt solution or 100 ppm of two types of dye solution was blended and used as feed solutions at 1 bar. The calculation of dye/salt selectivity (α) is shown below [25]:

$$\alpha = \frac{1 - Rs}{1 - Rd} \quad (4)$$

In addition, short-time stability measurement was conducted at 1 bar with DR23 solution for 50 h. The water permeability and dye retention were recorded every once in a while.

2.6. Adsorption capacity of GO/iCONs membranes

Adsorption measurement were proceeded to study the adsorption capacity of the GO/iCONs membranes to the objective dye. Briefly, the M3 and pure GO membrane were separately immersed into DR23 aqueous solution (200 mg L^{-1}) and subsequently fixed onto an incubator shaker (150 rpm, 25 °C) at least 6 h to achieve adsorption equilibrium. The adsorption capacity (q_e, mg/g) of the membranes is calculated according to the following equation [26]:

$$q_e = \frac{C_0 - C_e}{M} \times V \quad (5)$$

where C_o and C_e are the initial and equilibrium concentrations of DR23 (mg L^{-1}); V (L) refers to the volume of dye solution; M (g) is the mass of immersed GO/iCONs membranes.

2.7. Antimicrobial experiment

The plate count approach is employed to investigate antimicrobial property of the as-prepared membranes. Escherichia coli (*E. coli*) was chosen as the typical bacteria. Briefly, all the relevant items were sterilized with the aid of an autoclave prior to bacterial cultivation. The pristine bacterium fluid (200 μL) was decanted into a tube including sterile Luria-Bertani medium (10 mL) to cultivate at 37 °C at least 5 h. Subsequently, the samples were added to the suspension of E. coli for 2 h. Afterwards, the diluted suspension was coated onto solidified agar plates and breeded at 37 °C for overnight. Finally, the quantity of colonies was confirmed to assess the antimicrobial activity of GO/iCONs membranes.

2.8. Density functional theory (DFT) and molecular dynamics (MD) simulations

For the adsorption of iCONs precursor on a graphene monolayer, all ab initio total energy calculations were proceeded on account of density functional theory (DFT) within the framework of VASP (Vienna Ab initio Simulation Packages) code which uses a plane wave basis set for the electronic orbitals [27]. The electronic exchange and correlation was described within the generalized gradient approximation using the Perdew-Burke-Ernzerhof functional [28]. The interaction of the valence electrons with the ionic cores was treated within the projector augmented-wave (PAW) approach [29]. A large supercell was modeled with a cubic box of 12.30 Å × 12.78 Å × 18.8 Å. The original distance between two graphene layers are set to 8.38 Å obtained from XRD experimental data. A Monkhorst-Pack grid was used by K-points 2 × 2 × 1. The cut-off energy was employed as 450 eV. An electronic smearing was introduced within the Methfessel-Paxton scheme with σ = 0.1 eV. The interaction energy is defined as Ei=(E (Graphene + n × iCONs)-E (Graphene)-n × E (iCONs))/n, where E (Graphene) and E (iCONs) are the energies of graphene and iCONs, n is the number of iCONs [30].

MD simulations are implemented by the Forcite in the Material Studio software. The interatomic interactions are described by the force field of a condensed phase optimized molecular potential for atomistic simulation studies (COMPASS). COMPASS is a parameterized, tested and validated first ab initio force field, which enables accurate and simultaneous prediction of various gas-phase properties and condensed-phase properties of most of common organic and inorganic materials. All full atomistic simulations are subject to an NVT ensemble, and the temperature of the system is controlled by the Andersen thermostat method, with a fixed time step of 1 fs. Periodic boundary conditions are applied in the x and y directions. Two GO sheets (24.25 Å × 63 Å) serves as a GO membrane and the carbon-carbon opening of the slit is fixed at 8.52 Å. The interlayer spacing, which is defined as the vertical distance between upper and lower basal planes of GO sheets, is fixed at 8.38 Å. This is consistent with the experiment. The GO membrane separates a mix of water, dyes and Na_2SO_4 (consisting of 600 water molecules, 60 Na, 30 SO_4 and 3 dye molecules), chemical structures shown in Fig. S4. At the left of the feed phase, a wall composed of helium atoms is applied to hinder gas molecules passing to the vacuum phase due to the periodicity along the Z axis. During the simulation, the wall composed of helium atoms and the GO membrane are fixed. To compare with the system with iCONs, another similar model is constructed. A COF nanosheet is fixed between two GO sheets. Because iCONs will make the interlayer spacing larger, the distance between two GO sheets is fixed at 10.00 Å. The other parameters are the same as the system without iCONs.

3. Results and discussion

3.1. Synthesis of iCONs

$TpTG_{Cl}$ (denoted as iCONs) were synthesized through Schiff base

condensation reaction between triaminoguanidinium chloride (TG_{Cl}) and 1,3,5-triformylphloroglucinol (Tp) proceeded in a sealed Pyrex tube at 120 °C, as displayed in Fig. 1a. The obtained sample is in the form of powder with reddish brown color (Fig. 2a) and presents superb dispersity without any agglomeration even after maintaining for one month in aqueous medium (Fig. 2b) on account of containing ionic backbone.[23] A classical Tyndall effect is also observed implying stable colloidal suspension for this period exhibited in Fig. 2b. The XRD pattern of iCONs shows a high consistency with that of simulated XRD exhibited in Fig. 1b. The first broad peak at $2\theta = 9.8°$ attributed to the 100 facet indicates low crystallinity. This may be owning to the presence of positively charged guanidinium units and chloride ions, which disturbes the π-π stacking interaction among the layers, thus destroying the crystallinity of the polymers. In addition, the main wide peak at $2\theta = 27.5°$ manifestes weak stacking interaction originated from ionic layers with sandwiched halide ions in the two-dimensional direction, suggesting the synthesized polymers could self-exfoliate to covalent organic nanosheets [22]. Besides, FTIR was employed to evaluate the chemical structure of iCONs in Fig. 2c. The stretch peaks of the carbonyl (1635 cm^{-1}) and primary amine (3315 cm^{-1}) of the precursors disappear, signifying that co–condensation reaction is completed. Meanwhile, the characteristic peaks at 1595 cm^{-1} and 1290 cm^{-1} represent C═C and C–N, respectively [31]. Moreover, structural information of the iCONs was attained from N_2 adsorption isotherms at 77 K depicted in Fig. 2d, where the resultant polymer displays Type-II reversible adsorption isotherm. The obtained iCONs possess a low BET surface area of 209.5 $m^2\ g^{-1}$, probably due to the undesirable layer stacking as well as pore clogging via the contrary anions. It is worth noting that there is no obviously incisive pore size distribution in that the pore structure is improperly channelled in Fig. 2e. The result conforms to the published work in which the exfoliation of 2D-CPP laminates into CONs resulted in the pores to be destroyed [32]. Furthermore, TGA was applied to investigate the thermal stability of the iCONs, demonstrating no distinct decomposition appeared until 250 °C in N_2 atmosphere in Fig. 2f. Meanwhile, the elemental mapping of iCONs illustrates that C, N, O and Cl elements are distributed evenly in Fig. 2g–h. The lateral size of Go is around 5–12 μm, as exhibited in Fig. 2i.

Additionally, the morphology of the iCONs was characterized via TEM and SEM (Fig. 1c–d), exhibiting transparent sheets with slight ripples and large horizontal size varied from nanometer to micrometer. The corresponding AFM image showed that the range of height profile was around 2.5–3 nm, indicating that the iCONs could be exfoliated into 3–4 layers (Fig. 1e). The considerably large sheet size as well as thin structure makes the iCONs appropriate for fabrication of layered membranes.

3.2. Morphological structure of the GO/iCONs membranes

The GO/iCONs hybrid membranes were facilely fabricated via vacuum-assisted filtration strategy as exhibited in Fig. 3a. The electrostatic attraction and hydrogen bonding avail to enhanced interaction between GO and iCONs laminates in Fig. 3a. Meanwhile, the mixed GO/iCONs membrane sustains intact without shedding through several foldings (Fig. 3b) because of the interactions amid the deposited GO/iCONs layer and the support [4], illustrating the exceptional elasticity and ruggedness of the GO/iCONs membrane. The cross-sectional SEM image displays an even, flat and successive GO/iCONs layer firmly attached onto the surface of nylon support in Fig. 3c. Moreover, the selective layer of GO/iCONs membrane was clearly visualized by TEM (Fig. 3d), which coincides with the SEM results.

Furthermore, as evinced in Fig. 4a, SEM surface of pure GO membranes possesses characteristic crumples, which is relevant to the interactions between water molecules and the hydrophilic functional groups of GO laminates as well as the stress forced by the process of vacuum-driven filtration [33]. It is also found that contorted transmission channels located on the pores of the nylon supports due to the superb flexibility of GO laminates [34]. As exhibited in Fig. 4d, the surface of the fabricated GO/iCONs membranes have analogous crumples to those of GO membranes. With the rise of iCONs loading (Table S2), the slight aggregation of iCONs is detectable on the surface of the corresponding GO/iCONs membranes (Fig. 4g and j). While the iCONs loading is over 0.05 mg, larger aggregates of iCONs are discovered in Fig. 4m and p. This phenomenon is possibly due to state transition at diverse mass ratios employed in membrane preparation, that is,

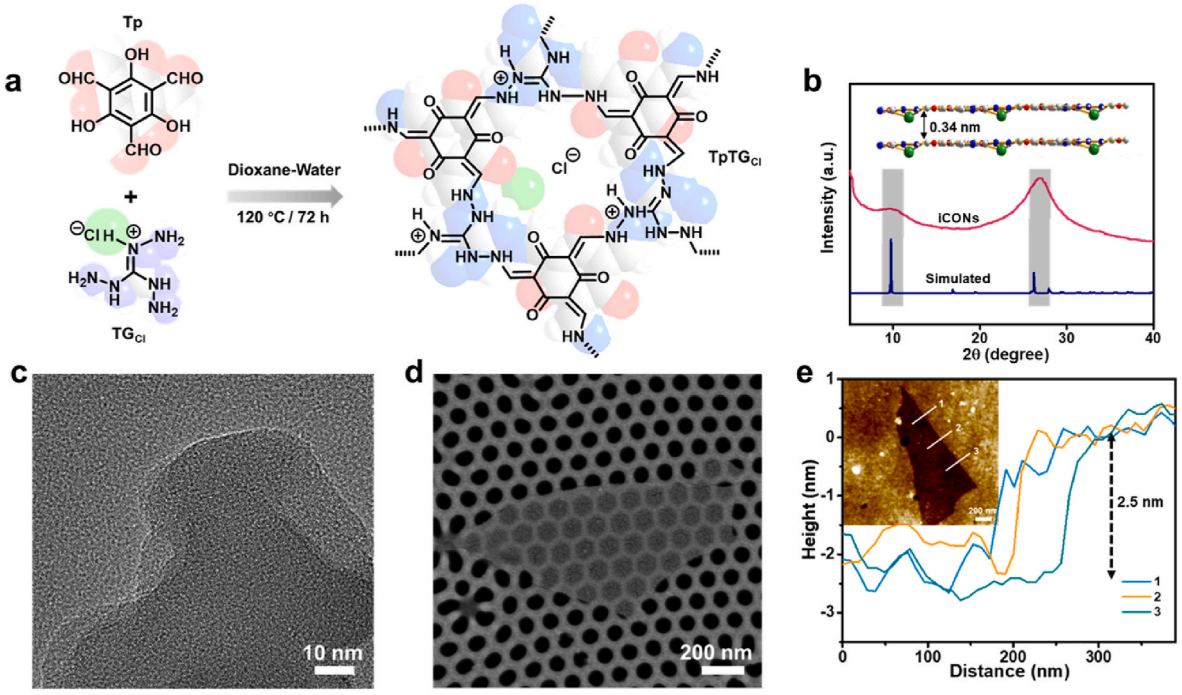

Fig. 1. (a) Synthetic scheme of iCONs, (b) XRD patterns, (c) TEM image, (d) SEM image, (e) AFM image on a silicon wafer (top left corner) and its thickness profile. (For interpretation of the references to color in this figure legend, the reader is referred to the Web version of this article.)

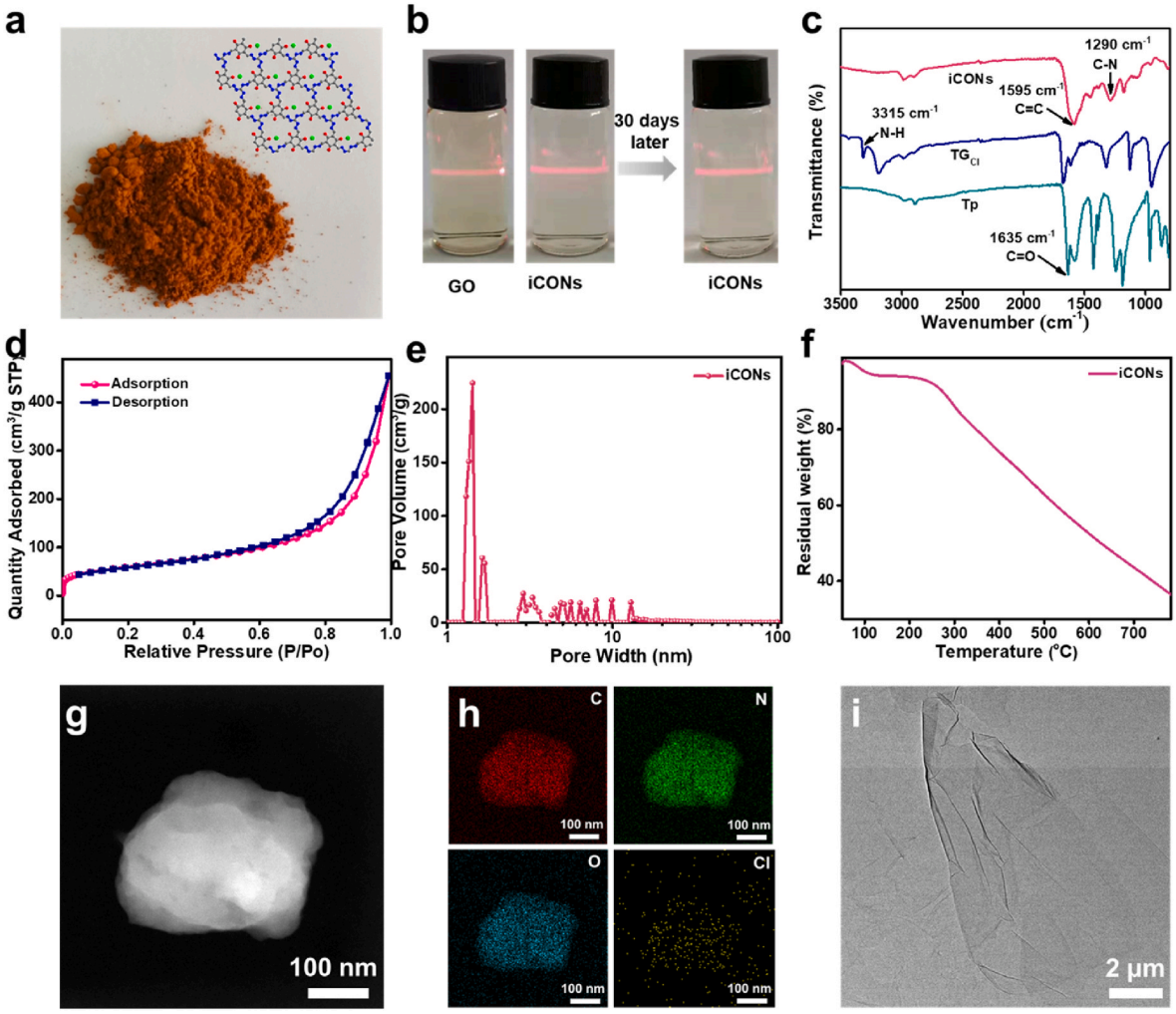

Fig. 2. (a) Digital photo of iCONs powder (inset: a simulated molecular structure of iCONs), (b) Tyndall effect demonstrates excellent dispersity of GO and iCONs in DI water, (c) FTIR spectra, (d) N_2 adsorption−desorption isotherms, (e) pore size distribution histogram calculated from N_2 adsorption, (f) thermogravimetric analysis result of iCONs powder, (g) TEM image of iCONs, (h) corresponding EDS-mapping images of iCONs, (i) TEM image of GO.

COFs is converted from nanosheets into aggregated particles as the concentration of iCONs boosts in aqueous dispersion [35]. In addition, the thickness of active layers for GO/iCONs membranes is of crucial importance for the sieving property. The thickness of original GO membrane is about 35 nm. With the increase of iCONs loading, the thickness of active layers slightly augments from 41 nm to 72 nm, as exhibited in Fig. 4f, i, l, o, r and Fig. 3e. The variations of thickness imply that the fabricated GO/iCONs membranes preserve dense stacked structures and the interlamellar spacing amid GO nanosheets is moderately expanded due to the intercalation of the iCONs, which will have an evident effect on the property of the fabricated laminar membranes. Moreover, surface roughness of the GO/iCONs membranes was explored via the AFM characterization. The 3D AFM images of GO/iCONs membranes with diverse iCONs loading were exhibited in Fig. 4e, h, k, n, q. The light color represents a high position on the membrane surface and the dark color refers to valleys or membrane pores [36]. The original GO membrane displays mildly peaks and valleys (Fig. 4b). After intercalation of the iCONs, the average roughness (Ra) of the fabricated GO/iCONs membranes increases, implying the formation of a comparatively rough surface in Fig. 4e, h, k, n, q, conforming to the results of SEM images.

3.3. Physicochemical, hydrophilicity, charge properties of the GO/iCONs membranes

The role of iCONs insertion on the interlamellar spacing of GO/iCONs membranes was firstly investigated by XRD in Fig. 5a. Note that the membranes were measured under a dry state to eliminate the influence of hydration. The characteristic peak of the GO membrane displays at 10.55°, which converts to layer spacing of 8.38 Å. The peak of GO/iCONs membranes marginally shifts to a lower theta at 9.25°, implying that the mean interlayer distance is augmented from 8.38 to 9.59 Å. Meanwhile, DFT was also applied to simulate the bonding effect and the results are as follows in Fig. 5b. The bond energy (electrostatic interaction and hydrogen bond) formed through GO and iCONs is stronger than that of π-π bonds amid the GO membrane. The average interlamellar spacing of pristine GO membrane is about 7.94 Å. The interlayer interaction energy of GO intercalated with iCONs is 3.09 eV and the d-spacing rises to 9.29 Å. The monolayer of GO and iCONs has an interlayer interaction energy of 2.13 eV, and its d-spacing lessens to 4.52 Å. The results of simulated layer spacing are basically consistent with those of XRD. Therefore, when iCONs were intercalated into the GO channels, they serve as a spacer to expand the size of channels amid GO laminates, promoting the transmission of water molecules in the channels. Additionally, the chemical constitute of the pristine GO membranes and GO/iCONs membranes was characterized by FTIR in Fig. 5c. FTIR

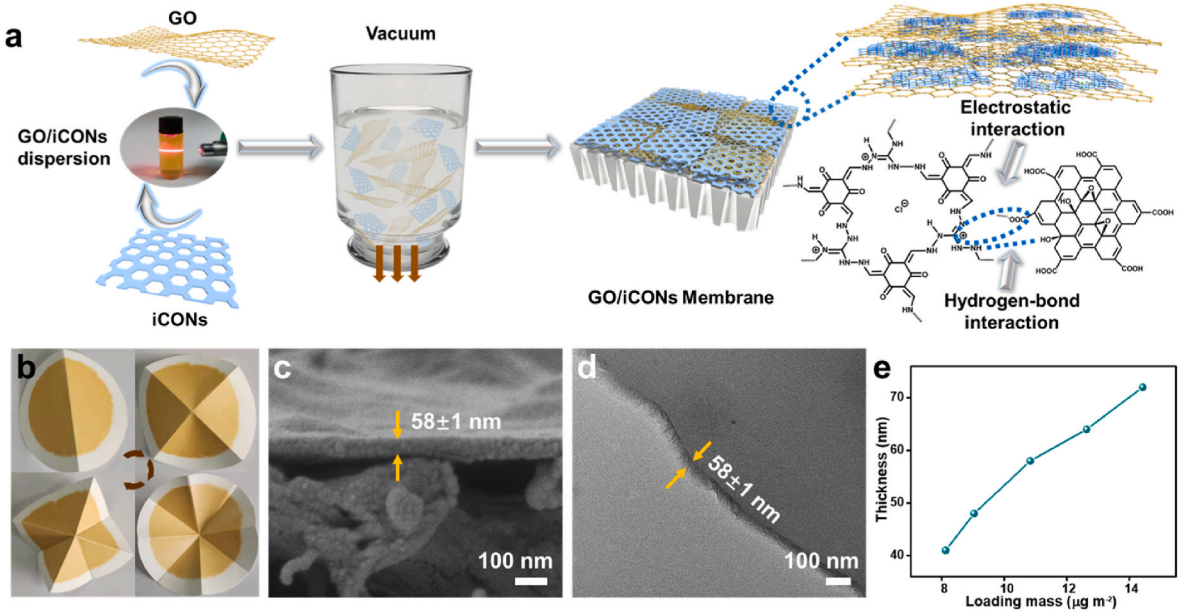

Fig. 3. (a) Schematic illustration of fabrication of GO/iCONs laminar membranes through vacuum-assisted filtration approach and interactions between GO and iCONs, (b) photographs of M3 after several folds, (c) cross-sectional SEM image of membrane (M3), (d) cross-sectional TEM image of M3, (e) relationship between the loading content of GO/iCONs and the thicknesses of the GO/iCONs hybrid membranes.

spectra of GO/iCONs membranes show a decrease in the intensity of carboxyl (1726 cm^{-1}) compared to GO membrane. Furthermore, GO/iCONs membranes exhibited new bands at 1582 cm^{-1}, verifying that the antisymmetric C–N stretching vibrations coupled with out-of plane NH modes [37]. These results demonstrated that iCONs was chemically linked with GO via C–N covalent bonds.

The surface wettability is a vital trait that influences the water permeance as well as antifouling property of the fabricated membranes [38]. The water contact angles (WCAs) of the GO/iCONs membranes are exhibited in Fig. 5d. It exhibits an obvious downward trend in the WCAs of the GO/iCONs membranes in comparison with pure GO membranes, indicating a higher surface hydrophilicity after the intercalation of iCONs, which avails to the rapid transport of water molecules. This is mainly attributed to the imino-containing iCONs possessing superb wettability. Additionally, the surface charge property of membrane is in connection with the chemical construction and has a critical effect on dye and salt retentions [39]. As evinced in Fig. 5e, the introduction of iCONs renders the GO/iCONs membranes less negatively charged in comparation with pristine GO laminar membranes. The GO/iCONs membranes still possess negative zeta potentials in the pH scope of 3.5–10. Furthermore, with the iCONs content raised, the negative charge of the GO/iCONs membranes mildly diminish. These results may be the result of complementary electrostatic interaction between the positively charged guanidine units within iCONs and the carboxyl group on GO nanosheets.

3.4. Separation property

The separation performances (water permeance and dye rejections) of the as-prepared membranes were assessed by using the pressure-driven cross-flow device as depicted in the experimental part. As exhibited in Table S3, pure GO laminar membranes with the loading mass of 0.1 mg have the water permeance as low as 17.8 L m^{-2} h^{-1} bar^{-1}. It can be ascribed to barrier effect of GO nanosheets, that is, interlayer channels are the sole transmission route for the layered GO membranes without pores [40], which yet possess preferable dye retentions (EBT, DR23, RB5, MB, MO is 99.8 %, 99.9 %, 98.8 %, 97.7 % and 66.4 %, respectively). After the intercalation of iCONs, the water permeation of GO/iCONs layered membranes obviously increases in Fig. 6a. The water permeation of M1 ascends to 73.6 L m^{-2} h^{-1} bar^{-1} and achieves 206.8 L m^{-2} h^{-1} bar^{-1} in M3 almost without sacrificing dye retentions in Figs. S2b–f, which is about 11-fold improvement over that of the pristine GO membranes. Reasonable causes are described below. Firstly, the insertion of iCONs can expand interlayer distance of GO nanosheets and thereby affording additional transmission channels. Secondly, the existence of iCONs pores with vertical alignment facilitates a higher flux. Thirdly, the insertion of the rigid iCONs into flexible GO nanosheets are possibly in favor of generating additional transmission paths. Hence, the existence of these multipaths within GO/iCONs layered membranes makes a critical difference in the enhancement of water flux. Nonetheless, the water permeation of GO/iCONs membranes dramatically declined with further augment of iCONs loading amount (M4 and M5). This may be caused by excessively adding iCONs, which leads to the agglomerations amid the interlamination cracks and 'edge-to-edge' stacking, thus forming a primary hindrance against the transport of water molecules [24]. Additionally, the thickness of the GO/iCONs membranes augments with the increase of iCONs content, which also results in additional transport resistance. Notably, M5 exhibits the most serious iCONs agglomeration, bringing about an unsatisfactory selectivity, illustrated in Fig. 4p.

As evinced in Fig. 6b, the salt retention of the GO/iCONs membranes follows the order Na_2SO_4 > $MgSO_4$ > NaCl > $MgCl_2$, which conforms to the sequence of the negatively charged membranes. Moreover, M3 exhibits relatively low retention (9.8 %, 8.1 %, 4.4 %, 1.9 % for Na_2SO_4, $MgSO_4$, NaCl, $MgCl_2$, respectively), and other membranes also generally display the low retention below 23.4 %. Therefore, the M3 possessing an ultra-high water permeance of 206.8 L m^{-2} h^{-1} bar^{-1}, excellent dye retention (97.4 %) as well as poor salt retention (<9.8 %) indicates great potential for the fractionation of dye/salts. Meanwhile, the DR23/salts permeance and selectivity of M3 were shown in Figure S3a and Fig. 6c. The dye permeance slightly declines on account of the forming of dye coating induced by adsorption and rejection of dye molecules onto the membrane surfaces. The M3 laminar membrane exhibits relatively high selectivity of DR23 and diverse salts (>33.6 %), peculiarly for DR23/Na_2SO_4, probably due to electrostatic repulsion [36]. Additionally, the mixtures of DR23/MO, RB5/MO and DR23/RB5 were separately filtrated through M3 to estimate molecular sieving property. The detailed information of used dye molecules is given in Table S4. When the hybrid

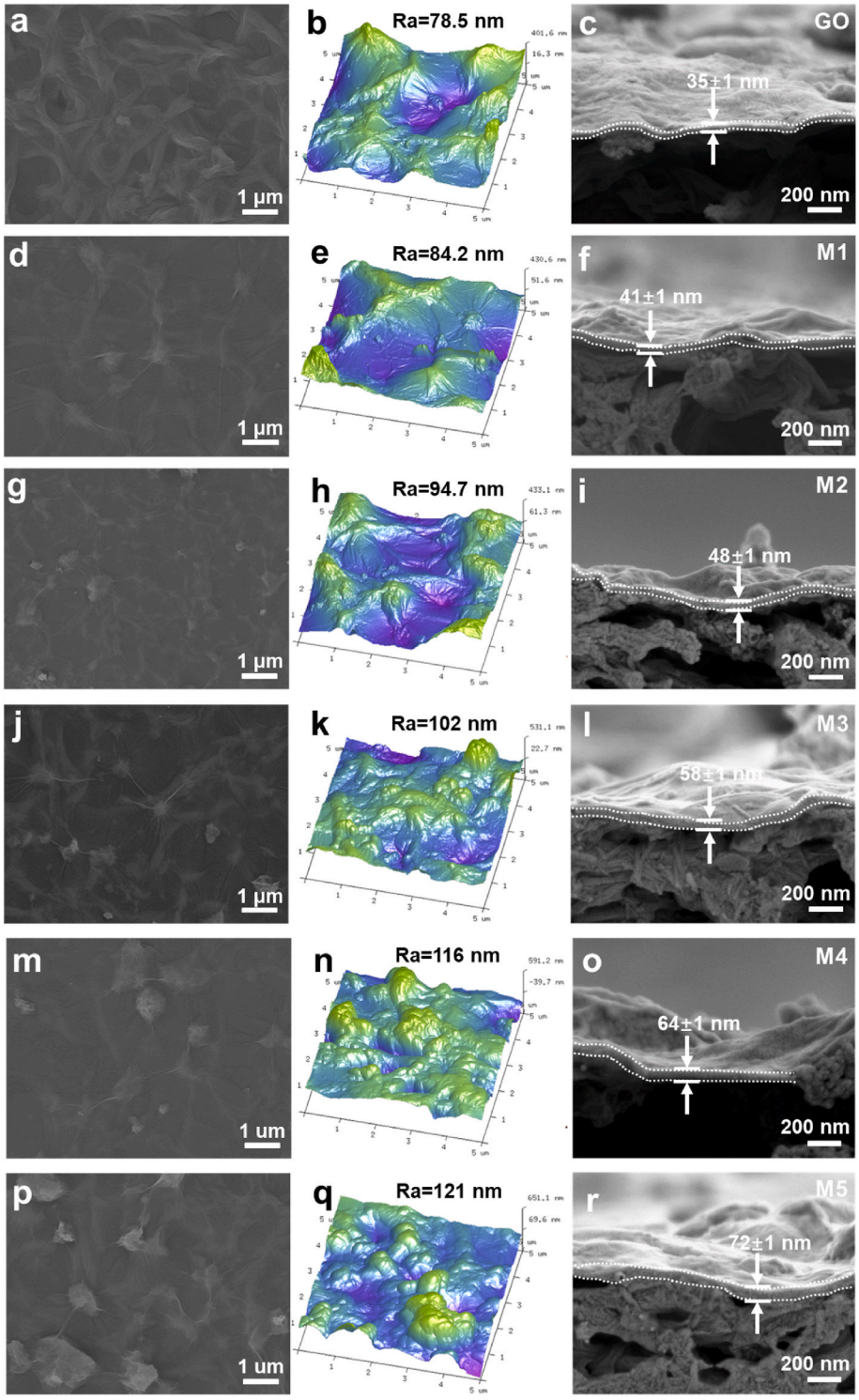

Fig. 4. SEM images of membrane surface (a, d, g, j, m, p), 3D AFM images (b, e, h, k, n, q) and cross-sectional SEM images of membranes (c, f, i, l, o, r). (a–c) GO, (d–f) M1, (g–i) M2, (j–l) M3, (m–o) M4, (p–r) M5.

feed originating from DR23/MO or RB5/MO is filtrated via the layered membrane in Fig. 6d and Figs. S3b and a yellow permeate is acquired by virtue of the primary channels of the MO molecules. Meanwhile, the UV–vis spectra manifest that M3 is equipped to reject DR23 or RB5, while the MO molecules can easily pass through. The superb molecular sieving ability of GO/iCONs membranes (that is, DR23/MO (31.4), RB5/MO (15.9) in Fig. S3c) is perhaps owning to the electrostatic repulsion between the electronegative dye molecules and negatively charged membrane surface. Besides, the mixed dyes (DR23/RB5) can be effectively removed through M3 (Fig. S3d), indicating its promising application in actual treatment of dyeing wastewater.

Furthermore, the short-term stability of M3 was also assessed after 50 h of operation, and the results are exhibited in Fig. 6e. Compared to the original water permeance (206.8 L m^{-2} h^{-1} bar^{-1}), the dye permeance of M3 was reduced. This may be caused by the gathering of a small amount of DR23 molecules on the membrane surface. As known,

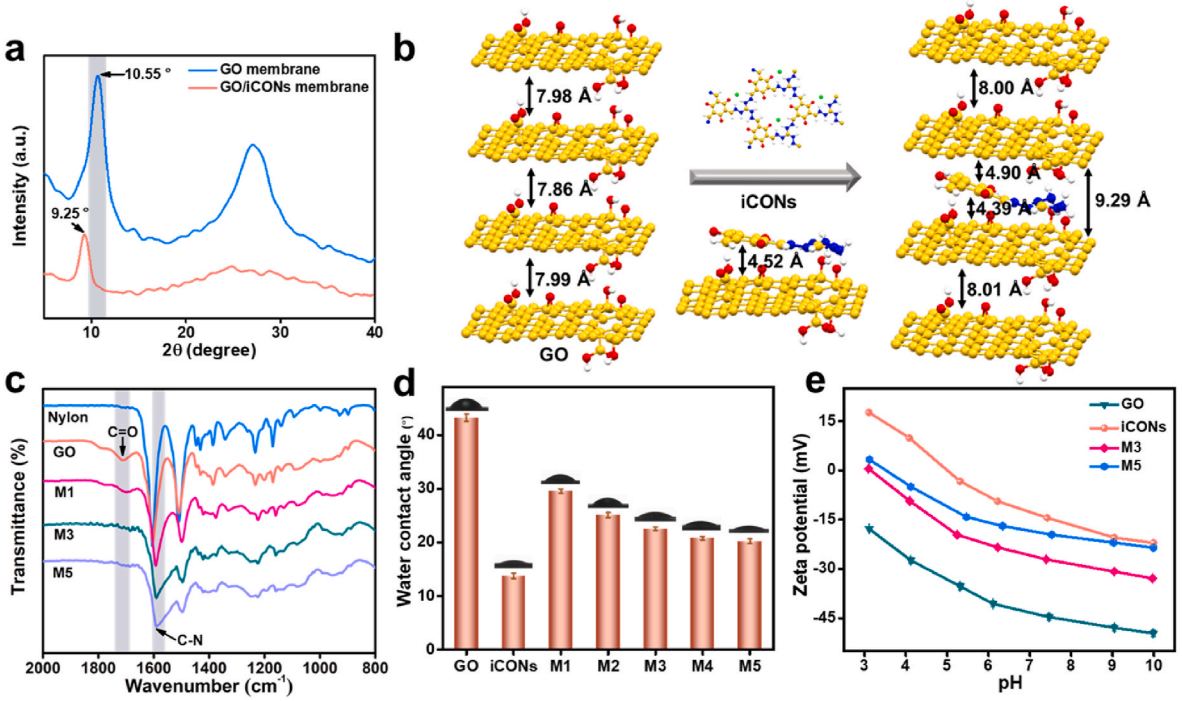

Fig. 5. (a) XRD curves, (b) DFT simulations of the GO-iCONs membrane, (c) FT-IR spectra, (d) water contact angles of pure GO membrane and GO/iCONs membranes, (e) zeta potential values of pure GO membrane and GO/iCONs membranes.

the absorption process is dynamic since the dye molecules possess excellent water solubility. Therefore, the dye permeance (~173.9 L m^{-2} h^{-1} bar^{-1}) tends to be stable without sacrificing dye retention (~98.0 %) when the adsorption equilibrium is achieved. The results also demonstrates that these membranes have the outstanding robustness as a result of the GO nanosheets intercalated with iCONs. Besides, the property of the GO/iCONs laminar membranes and other layered membranes is listed in Table S5. Compared with other fabricated membranes, the results indicate that the thus-obtained laminar membranes prepared in this study show an exceptional water permeance and preferable dye retentions, illustrated in Fig. 6f.

Additionally, to further explore water or ion transport property, MD simulations using two models were proceeded: pure GO membrane and GO/iCONs membrane. Abundant water passed through the GO/iCONs layered membranes was discovered in Fig. 6g. Furthermore, the results reveal that the water molecule or sodium salt could pass through GO/iCONs membrane fast, yet much more slowly through pure GO membrane (Fig. 6h), which is consistent with experimental results (Fig. 6a). Owning to the insertion of iCONs nanosheets, the limited channels necessarily display an enhanced interlamellar spacing compared with pure GO membranes, as manifested through XRD (Fig. 5a). The MD simulations also illustrate that the intercalated iCONs with pores can generate ultra-fast water transmission channels and high salt rejection. Furthermore, some gaps or cracks are formed between iCONs and GO laminates, which adds extra water channels to afford higher water permeance.

3.5. Antimicrobial property and stability of the GO/iCONs membranes

Membrane biofouling is an important aspect that severely influences the separation efficiency and the operational stability of water-based membranes. Previous researches reported that the membrane with a neutral and smoothly hydrophilic surface had been demonstrated to possess an ultra-low tendency of bacteria attachment [41]. Nonetheless, in the long-term operation process, the attached bacteria would grow and multiply again, which resulted in serious membrane biofouling. Hence, an efficacious strategy is to design functionalized membranes possessing antimicrobial characteristic with nanomaterials like iCONs, which could inactivate or kill bacteria prior to they adhere to the surface [42]. In virtue of plate counting method, the bacterial activity after being touched with membrane samples is illustrated in Fig. 7a–f. Compared with the blank nylon membranes, the number of survivable *E. coli* colonies of the pure GO and iCONs membranes sharply declines, which evinces these two pure materials can effectively remove membrane biofouling. The pristine GO membranes have a bacteriostasis rate (BR) up to 80.5 % (Fig. 7g), which is possibly due to the mechanisms of sharp edges of GO and oxidative stress (ROS) [43]. Meanwhile, the iCONs membranes are found to possess a high degree of antibacterial activity (82.7 %). For one thing, positively charged iCONs could interact with bacterial cells followed by the destruction of negatively charged phospholipid bilayer. This would lead to leaching out of the cellular content and subsequently death of the bacteria. For another, hydrogen bonding interaction between the keto groups of iCONs and phospholipids is likely to avail for the antimicrobial mechanism [44]. Furthermore, the BR of the GO/iCONs composite membranes raise up to 98.5 %, which proves a preferable sterilization ability primarily stemming from the synergistic effect of iCONs and GO laminates. The antimicrobial mechanism of the GO/iCONs membranes is exhibited in Fig. 7h.

Stability is defined as the trend of layered membranes to keep integrated and preserve main geometry against external interferences, including dynamic (e.g., vigorous crossflow) or static (e.g., swelling) mode. Adequate stability is the precondition to sustain transmembrane nanofluidic transport and predict membrane property in practice, which can be acquired via incorporating appropriate guest materials [45]. As demonstrated in Fig. 8, the stability of GO-related membranes in DI water were estimated. Long-range touch with DI water results in the redispersion of GO nanosheets, following by the segregation of GO nanosheets from the supports, which is in line with the previous reports [21]. Contrary to pure GO membranes, the hybrid assembly of iCONs and GO imparts an obviously enhanced structural robustness of GO/iCONs layered membranes, which can maintain the same appearance after being immersed in water for more than 30 days. The plausible

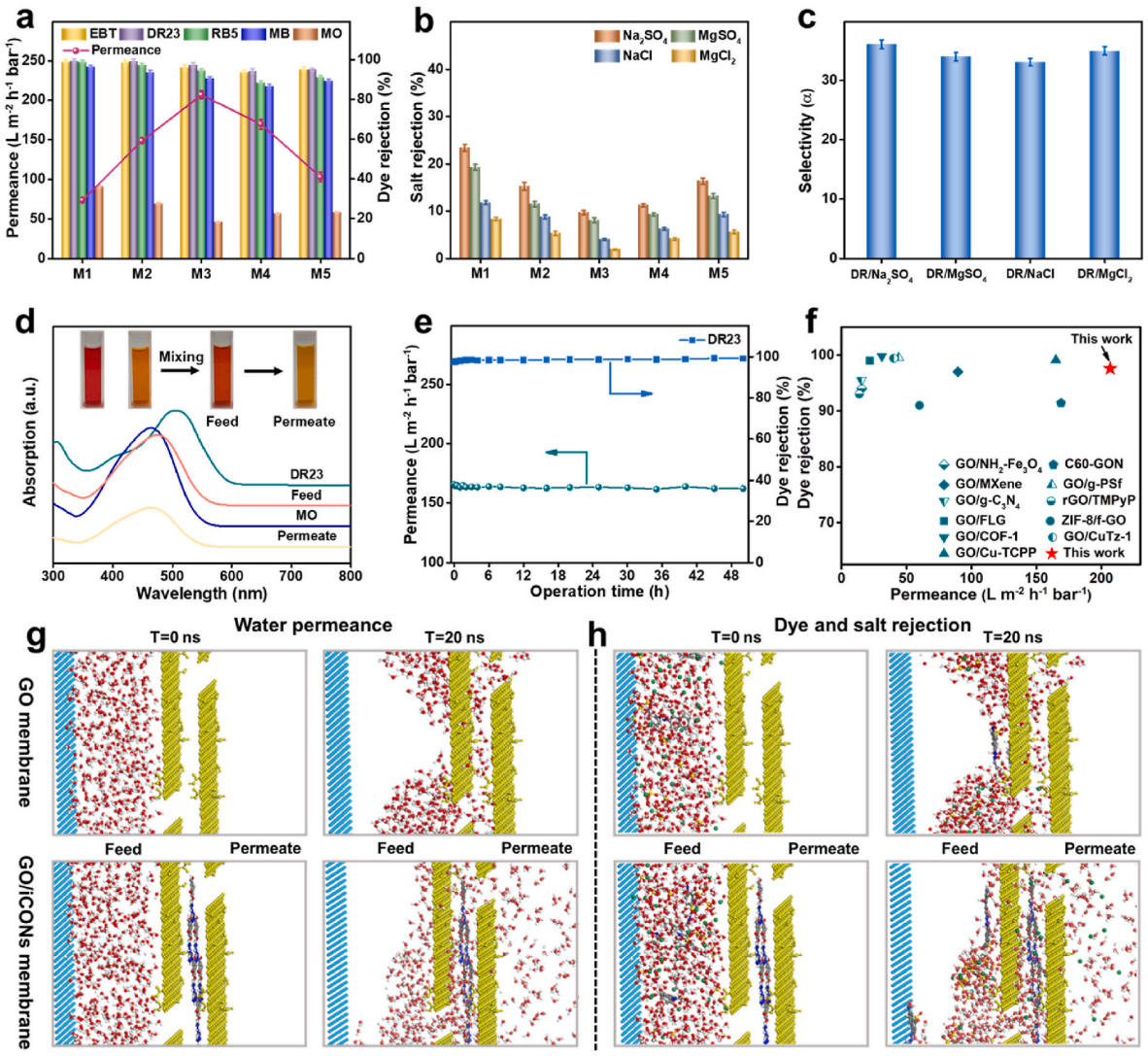

Fig. 6. (a) Permeance and dye rejection of GO/iCONs laminar membranes with diverse mass ratios, (b) salt rejection of GO/iCONs laminar membranes with diverse mass ratios, (c) DR23/salts selectivity of M3, (d) UV–Vis spectrum of diverse dye solutions and separation of DR23/MO in aqueous solution via a cross-flow device, (e) short-time stability test of M3 using DR23 (0.2 g L^{-1}) under 1 bar. (f) dye rejections of GO/iCONs membrane (M3) in comparison with those of other GO-based membranes. MD simulation snapshots at 0 ns and 20 ns for two systems: pure GO membrane and GO/iCONs membrane. Water permeance (g) and rejection of solutes (h) are simulated.

explanations for the excellent stability of GO/iCONs hybrid membranes are as below. For one thing, the insertion of iCONs laminates impairs the charge on the GO nanosheets in Fig. 5e. For another, electrostatic attraction exists in the interaction between the positively charged guanidine units within iCONs and the negatively charged GO membranes. Besides, the weak interaction including hydrogen bonding avails to an enhanced interaction between GO and iCONs laminates in Fig. 3a [46].

4. Conclusions

In summary, we demonstrated “complementary nanosheets” tactic for the facile assembly of precise-sieving, ultrathin, and defect-free GO-based layered membranes, displaying high permeance and attractive structural robustness for desalination in virtue of vacuum-assisted filtration approach. This physicochemically complementary nanosheets assembly was proved to stabilize the layered GO-based membranes, which could efficaciously prevent swelling in the water. This is primarily ascribed to electrostatic attraction and hydrogen bonding interaction between iCONs and GO nanosheets. Furthermore, the insertion of iCONs laminates amid the GO nanosheets allows for expanding interlayer spacing to improve water permeance. The inherent pores and interfacial gaps as extra water channels are also in favor of enhancing water permeance in comparation with that of pure GO membranes. Additionally, the high dye retention and low salt rejection enable GO/iCONs membranes quite appropriate for dye purification. Furthermore, the fabricated membranes allow for precise molecular sieving among DR23/MO, RB5/MO and DR23/salts. Moreover, the superb antimicrobial property of GO/iCONs membranes is achieved owing to synergistic effect of GO and iCONs, which is primarily attributed to electrostatic effect produced by positively charged guanidine units within iCONs and sharp edges and ROS generated by GO nanosheets. Overall, this study illustrates the role of intercalated iCONs in laminar GO membranes and affords a complementary protocol to design a porous and water stable 2D materials, which offer fast water transport channels for next generation of GO-based membrane separation.

CRediT authorship contribution statement

Rui Li: Writing – original draft, Investigation, Data curation. **Xiaoquan Feng:** Validation, Investigation. **Huixian Wang:** Validation,

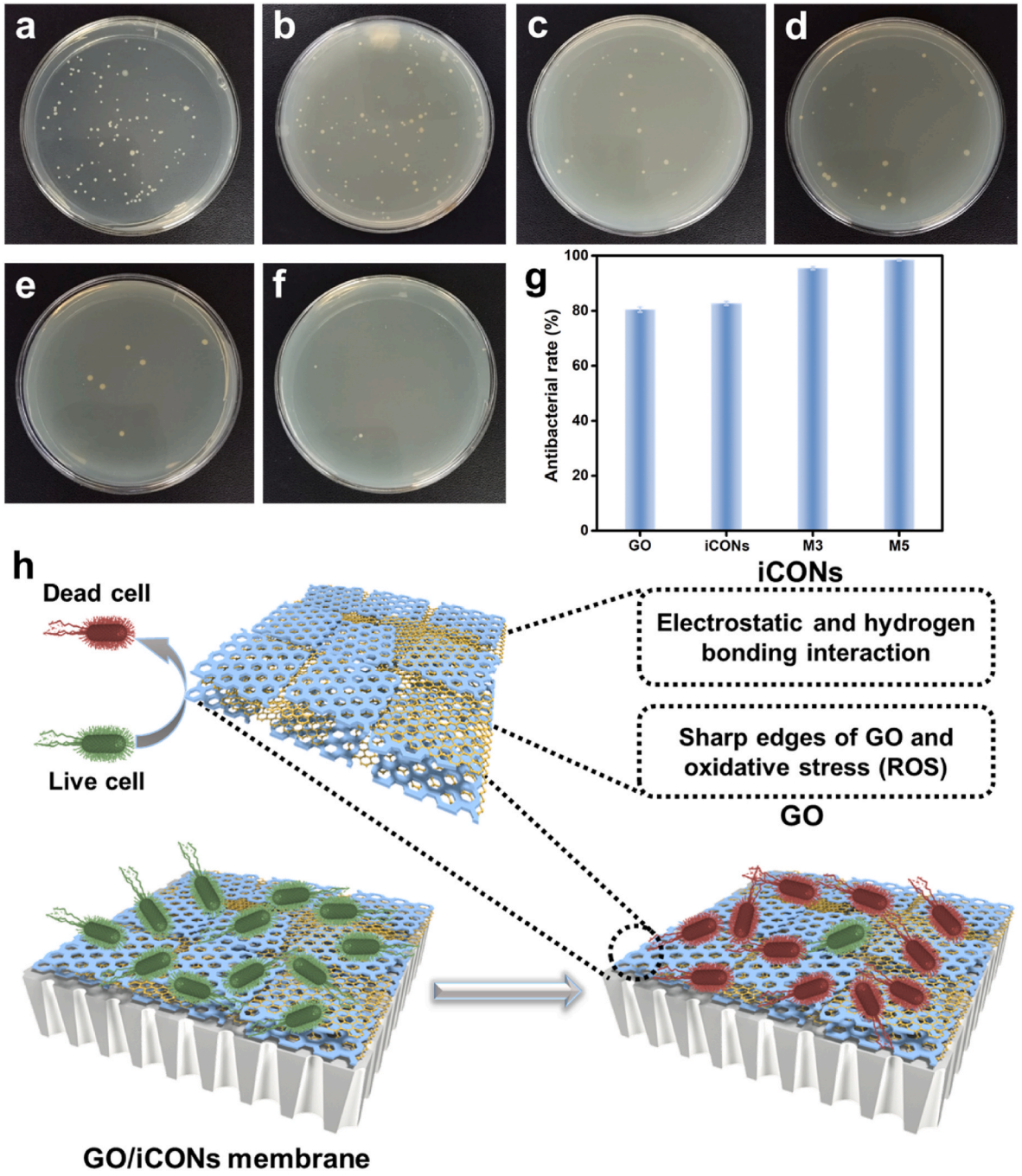

Fig. 7. Antibacterial ability of the membranes: (a) control, (b) nylon, (c) GO membrane, (d) iCONs membrane, (e) M3, (f) M5, (g) the antibacterial rate of GO, iCONs and GO/iCONs composite membranes (M3 and M5), (h) the proposed antimicrobial mechanism of the GO/iCONs composite membranes.

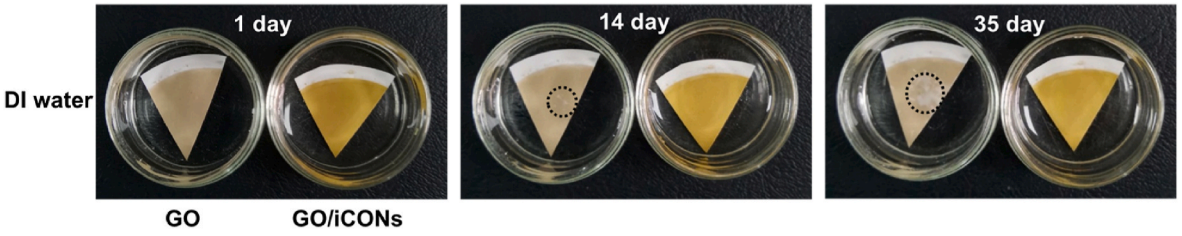

Fig. 8. Optical photos showing the stability of GO and GO/iCONs composite membranes in aqueous solution for 35 days standing.

Investigation. **Donglai Peng:** Validation. **Shaochong Cao:** Data curation. **Jingtao Wang:** Writing – review & editing. **Yatao Zhang:** Writing – review & editing, Supervision. **Yong Wang:** Writing – review & editing, Supervision.

Declaration of competing interest

The authors declare that they have no known competing financial interests or personal relationships that could have appeared to influence the work reported in this paper.

Data availability

Data will be made available on request.

Acknowledgements

This work was supported by Natural Science Foundation of Henan (222300420018) and Key Scientific Research Projects in Universities of Henan Province (21zx006 and 22B430018). The authors gratefully thank Center of Advanced Analysis & Computational Science, Zhengzhou University for help with the characterization.

Appendix A. Supplementary data

Supplementary data to this article can be found online at https://doi.org/10.1016/j.memsci.2024.122799.

References

[1] S.B. Kwon, Y. Kim, S. Lee, S. Hong, High-performance support-free molecular layer-by-layer assembled forward osmosis membrane incorporated with graphene oxide, J. Membr. Sci. 689 (2024) 122152.
[2] Y. Zhang, Y. Wang, X. Wang, Z. Zhang, S. Li, Y. Hu, G. Gong, Construction of robust one-dimensional nanowire-regulated graphene oxide membranes for efficient dye/salt separation, J. Membr. Sci. 686 (2023) 122027.
[3] F. Jia, X. Xiao, A. Nashalian, S. Shen, L. Yang, Z. Han, H. Qu, T. Wang, Z. Ye, Z. Zhu, L. Huang, Y. Wang, J. Tang, J. Chen, Advances in graphene oxide membranes for water treatment, Nano Res. 15 (2022) 6636–6654.
[4] Q. Lan, C. Feng, Z. Wang, L. Li, Y. Wang, T. Liu, Chemically laminating graphene oxide nanosheets with phenolic nanomeshes for robust membranes with fast desalination, Nano Lett. 21 (2021) 8236–8243.
[5] W. Zhang, H. Xu, F. Xie, X. Ma, B. Niu, M. Chen, H. Zhang, Y. Zhang, D. Long, General synthesis of ultrafine metal oxide/reduced graphene oxide nanocomposites for ultrahigh-flux nanofiltration membrane, Nat. Commun. 13 (2022) 471.
[6] I.A. Shah, M. Bilal, I.W. Almanassra, I. Ihsanullah, A comprehensive review of graphene oxide-based membranes for efficient dye removal from water sources, Sep. Purif. Technol. 330 (2024) 125277.
[7] F. Jia, L. Yang, L. Sun, D. Yu, Y. Song, Y. Wang, M.J. Kipper, J. Tang, L. Huang, Efficient separation of dyes using two-dimensional heterogeneous composite membranes, Water Res. 247 (2023) 120693.
[8] S. Rajesh, A.B. Bose, Development of graphene oxide framework membranes via the "from" and "to" cross-linking approach for ion-selective separations, ACS Appl. Mater. Interfaces 11 (2019) 27706–27716.
[9] B. Yuan, M. Wang, B. Wang, F. Yang, X. Quan, C.Y. Tang, Y. Dong, Cross-linked graphene oxide framework membranes with robust nano-channels for enhanced sieving ability, Environ. Sci. Technol. 54 (2020) 15442–15453.
[10] H. Liu, H. Wang, X. Zhang, Facile fabrication of freestanding ultrathin reduced graphene oxide membranes for water purification, Adv. Mater. 27 (2015) 249–254.
[11] A. Akbari, P. Sheath, S.T. Martin, D.B. Shinde, M. Shaibani, P.C. Banerjee, R. Tkacz, D. Bhattacharyya, M. Majumder, Large-area graphene-based nanofiltration membranes by shear alignment of discotic nematic liquid crystals of graphene oxide, Nat. Commun. 7 (2016) 10891.
[12] K. Goh, W. Jiang, H.E. Karahan, S. Zhai, L. Wei, D. Yu, A.G. Fane, R. Wang, Y. Chen, All-carbon nanoarchitectures as high-performance separation membranes with superior stability, Adv. Funct. Mater. 25 (2015) 7348–7359.
[13] M. Hu, B. Mi, Layer-by-layer assembly of graphene oxide membranes via electrostatic interaction, J. Membr. Sci. 469 (2014) 80–87.
[14] D.W. Kim, J. Choi, D. Kim, H.T. Jung, Enhanced water permeation based on nanoporous multilayer graphene membranes: the role of pore size and density, J. Mater. Chem. A 4 (2016) 17773–17781.
[15] L. Nie, K. Goh, Y. Wang, J. Lee, Y. Huang, H.E. Karahan, K. Zhou, M.D. Guiver, T.-H. Bae, Realizing small-flake graphene oxide membranes for ultrafast size-dependent organic solvent nanofiltration, Sci. Adv. 6 (2020) eaaz9184.
[16] W. Zhou, M.J. Wei, X. Zhang, F. Xu, Y. Wang, Fast desalination by multilayered covalent organic framework (COF) nanosheets, ACS Appl. Mater. Interfaces 11 (2019) 16847–16854.
[17] C.S. Diercks, O.M. Yaghi, The atom, the molecule, and the covalent organic framework, Science 355 (2017).
[18] J. Liu, G. Han, D. Zhao, K. Lu, J. Gao, T.S. Chung, Self-standing and flexible covalent organic framework (COF) membranes for molecular separation, Sci. Adv. 6 (2020) eabb1110.
[19] H. Fan, J. Gu, H. Meng, A. Knebel, J. Caro, High-flux membranes based on the covalent organic framework COF-LZU1 for selective dye separation by nanofiltration, Angew. Chem. Int. Ed. 57 (2018) 4083–4087.
[20] Z. Lei, Q. Yang, Y. Xu, S. Guo, W. Sun, H. Liu, L.P. Lv, Y. Zhang, Y. Wang, Boosting lithium storage in covalent organic framework via activation of 14-electron redox chemistry, Nat. Commun. 9 (2018) 576.
[21] Y. Liu, J. Guan, Y. Su, R. Zhang, J. Cao, M. He, J. Yuan, F. Wang, X. You, Z. Jiang, Graphene oxide membranes with an ultra-large interlayer distance through vertically grown covalent organic framework nanosheets, J. Mater. Chem. A 7 (2019) 25458–25466.
[22] S. Mitra, S. Kandambeth, B.P. Biswal, A. Khayum M, C.K. Choudhury, M. Mehta, G. Kaur, S. Banerjee, A. Prabhune, S. Verma, S. Roy, U.K. Kharul, R. Banerjee, Self-exfoliated guanidinium-based ionic covalent organic nanosheets (iCONs), J. Am. Chem. Soc. 138 (2016) 2823–2828.
[23] S. Cong, H. Li, X. Shen, J. Wang, J. Zhu, J. Liu, Y. Zhang, B. Van der Bruggen, Construction of graphene oxide based mixed matrix membranes with CO_2-philic sieving gas-transport channels through strong π–π interactions, J. Mater. Chem. A 6 (2018) 17854–17860.
[24] Z. Wang, J. Zhu, S. Xu, Y. Zhang, B. Van der Bruggen, Graphene-like MOF nanosheets stabilize graphene oxide membranes enabling selective molecular sieving, J. Membr. Sci. 633 (2021) 119397.
[25] A. Gopalakrishnan, M.L. Mathew, J. Chandran, J. Winglee, A.R. Badireddy, M. Wiesner, C.T. Aravindakumar, U.K. Aravind, Sustainable polyelectrolyte multilayer surfaces: possible matrix for salt/dye separation, ACS Appl. Mater. Interfaces 7 (2015) 3699–3707.
[26] S. Zhou, X. Feng, J. Zhu, Q. Song, G. Yang, Y. Zhang, B. Van der Bruggen, Self-cleaning loose nanofiltration membranes enabled by photocatalytic Cu-triazolate MOFs for dye/salt separation, J. Membr. Sci. 623 (2021) 119058.
[27] D. Jiang, M.H. Du, S. Dai, First principles study of the graphene/Ru(0001) interface, J. Chem. Phys. 130 (2009) 074705.
[28] K. Burke, M. Ernzerhof, J.P. Perdew, The adiabatic connection method: a non-empirical hybrid, Chem. Phys. Lett. 265 (1997) 115–120.
[29] C. Portalés, P. Casanova-Salas, S. Casas, J. Gimeno, M. Fernández, An interactive cameraless projector calibration method, Virtual Real. 24 (2020) 109–121.
[30] B.C. Melot, A. Goldman, L.E. Darago, J.D. Furman, E.E. Rodriguez, R. Seshadri, Magnetic ordering and magnetodielectric phenomena in $CoSeO_4$, J. Phys. Condens. Matter 22 (2010) 506003.
[31] S. Kandambeth, A. Mallick, B. Lukose, M.V. Mane, T. Heine, R. Banerjee, Construction of crystalline 2D covalent organic frameworks with remarkable chemical (acid/base) stability via a combined reversible and irreversible route, J. Am. Chem. Soc. 134 (2012) 19524–19527.
[32] S. Chandra, S. Kandambeth, B.P. Biswal, B. Lukose, S.M. Kunjir, M. Chaudhary, R. Babarao, T. Heine, R. Banerjee, Chemically stable multilayered covalent organic nanosheets from covalent organic frameworks via mechanical delamination, J. Am. Chem. Soc. 135 (2013) 17853–17861.
[33] Y. Wei, Y. Zhang, X. Gao, Y. Yuan, B. Su, C. Gao, Declining flux and narrowing nanochannels under wrinkles of compacted graphene oxide nanofiltration membranes, Carbon 108 (2016) 568–575.
[34] Y. Yuan, X. Gao, Y. Wei, X. Wang, J. Wang, Y. Zhang, C. Gao, Enhanced desalination performance of carboxyl functionalized graphene oxide nanofiltration membranes, Desalination 405 (2017) 29–39.
[35] X. Sui, Z. Yuan, C. Liu, L. Wei, M. Xu, F. Liu, A. Montoya, K. Goh, Y. Chen, Graphene oxide laminates intercalated with 2D covalent-organic frameworks as a robust nanofiltration membrane, J. Mater. Chem. A 8 (2020) 9713–9725.
[36] L. Qin, Y. Zhao, J. Liu, J. Hou, Y. Zhang, J. Wang, J. Zhu, B. Zhang, Y. Lvov, B. Van der Bruggen, Oriented clay nanotube membrane assembled on microporous polymeric substrates, ACS Appl. Mater. Interfaces 8 (2016) 34914–34923.
[37] J. Shen, G. Liu, K. Huang, Z. Chu, W. Jin, N. Xu, Subnanometer two-dimensional graphene oxide channels for ultrafast gas sieving, ACS Nano 10 (2016) 3398–3409.
[38] J. Wang, Y. Wang, Y. Zhang, A. Uliana, J. Zhu, J. Liu, B. Van der Bruggen, Zeolitic imidazolate framework/graphene oxide hybrid nanosheets functionalized thin film nanocomposite membrane for enhanced antimicrobial performance, ACS Appl. Mater. Interfaces 8 (2016) 25508–25519.
[39] Y. Liu, J. Zhu, J. Zheng, X. Gao, M. Tian, X. Wang, Y.F. Xie, Y. Zhang, A. Volodin, B. Van der Bruggen, Porous organic polymer embedded thin-film nanocomposite membranes for enhanced nanofiltration performance, J. Membr. Sci. 602 (2020) 117982.
[40] J. Ma, X. Guo, Y. Ying, D. Liu, C. Zhong, Composite ultrafiltration membrane tailored by MOF@GO with highly improved water purification performance, Chem. Eng. J. 313 (2017) 890–898.
[41] J. Zhu, J. Hou, Y. Zhang, M. Tian, T. He, J. Liu, V. Chen, Polymeric antimicrobial membranes enabled by nanomaterials for water treatment, J. Membr. Sci. 550 (2018) 173–197.
[42] J. Zhu, J. Wang, A.A. Uliana, M. Tian, Y. Zhang, Y. Zhang, A. Volodin, K. Simoens, S. Yuan, J. Li, J. Lin, K. Bernaerts, B. Van der Bruggen, Mussel-inspired architecture of high-flux loose nanofiltration membrane functionalized with antibacterial reduced graphene oxide-copper nanocomposites, ACS Appl. Mater. Interfaces 9 (2017) 28990–29001.
[43] F. Perreault, A. Fonseca de Faria, M. Elimelech, Environmental applications of graphene-based nanomaterials, Chem. Soc. Rev. 44 (2015) 5861–5896.

[44] H.L. Zhang, Y.-B. Gao, J.-G. Gai, Guanidinium-functionalized nanofiltration membranes integrating anti-fouling and antimicrobial effects, J. Mater. Chem. A 6 (2018) 6442–6454.
[45] Y. Kang, Y. Xia, H. Wang, X. Zhang, 2D Laminar membranes for selective water and ion transport, Adv. Funct. Mater. 29 (2019) 1902014.
[46] A.R. Monteiro, M.G.P.M.S. Neves, T. Trindade, Functionalization of graphene oxide with porphyrins: synthetic routes and biological applications, ChemPlusChem 85 (2020) 1857–1880.